CJC Chinese Journal of Chemistry 中国化学 · An International Journal

For submission: https://mc.manuscriptcentral.com/cjoc
For published articles: https://onlinelibrary.wiley.com/journal/16147065

Concise Report

Cite this paper: *Chin. J. Chem.* **2022**, *40*, 2428—2436. **DOI: 10.1002/cjoc.202200334**

Co-delivery of Cisplatin and Chlorin e6 by Poly(phosphotyrosine) for Synergistic Chemotherapy and Photodynamic Therapy

Haisen Zhou,[‡,a] Yaoyi Wang,[‡,a] Yingqin Hou,[a] Zhengkui Zhang,[b] Qi Wang,[b] Xiaodong Tian,*[,b] and Hua Lu*[,a]

[a] *Beijing National Laboratory for Molecular Sciences, Center for Soft Matter Science and Engineering, Key Laboratory of Polymer Chemistry and Physics of Ministry of Education, College of Chemistry and Molecular Engineering, Peking University, Beijing 100871, China*
[b] *Department of General Surgery, Peking University First Hospital, Beijing 100034, China*

Comprehensive Summary

Nanoscale drug delivery systems (NDDSs) have emerged as promising carriers for combinational therapy by co-delivery of multiple drugs and modalities. However, most co-delivery systems require the use of complicated materials and formulations. Herein, we report the single use of a polymeric material, namely mPEG-*block*-poly(phosphotyrosine) (mPEG-*b*-PpY), as a multi-functional carrier for the facile fabrication of NDDS Pt/Ce6@mPEG-b-PpY (PtCeNP) for the co-delivery of cisplatin and photosensitizer chlorin e6 (Ce6) via phosphato-platinum coordination and π-π stacking, respectively. PtCeNP improves the solubility, cellular uptake, and bioavailability of both parental drugs, and showed strong synergistic antitumor efficacy both *in vitro* and *in vivo* through combined chemo-photodynamic therapy. Our results indicate that PpY is a biocompatible, multifunctional, and promising carrier material suitable for a variety of drugs and may simplify the design for co-delivery systems.

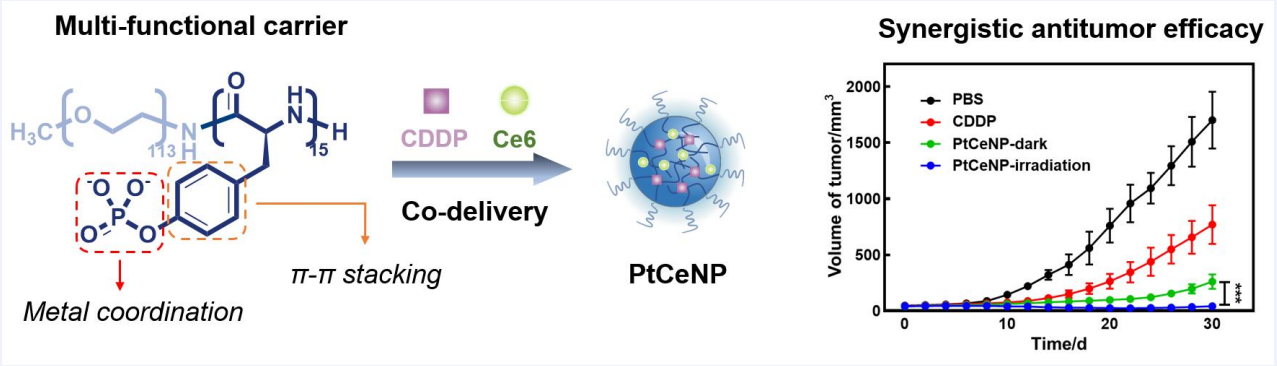

Keywords

Drug delivery | Poly(phosphotyrosine) | Block copolymers | Nanoparticles | Combinational chemo-photodynamic therapy

*E-mail: chemhualu@pku.edu.cn; tianxiaodong@pkufh.cn
‡ These authors contributed equally.

View HTML Article | Supporting Information

Background and Originality Content

Chemotherapy has played an important role in the fight against cancer. However, traditional chemotherapeutics often cause severe systemic side effects and re-occurrence of tumors owing to nonspecific drug accumulation, low bioavailability, and drug resistance.[1-2] On the contrary, photodynamic therapy (PDT) produces spatiotemporal controllable cytotoxic reactive oxygen species (ROS) generated by photosensitizers upon light irradiation, which can kill tumor cells with less damage to the surrounding tissues.[3-7] Nevertheless, most photosensitizers are aromatic compounds with low aqueous solubility and poor bioavailability, which restrict their application in clinical use.[8-9] In addition, due to the heterogeneity of tumor tissues, a single treatment modality usually cannot completely eliminate the tumor, resulting in poor prognosis.[10-11] As such, combined chemo-photodynamic therapy has been developed in recent years to reduce side effects and improve treatment outcomes.[12-20] However, simple bolus administration of chemotherapeutics and photodynamic therapeutics cannot achieve sustained synergistic therapeutic effects due to differential pharmacokinetics, biodistribution, and metabolism profiles of the drugs.[21] Thus, various types of nanoscale drug delivery systems (NDDSs), such as liposomes,[22-23] polymeric micelles,[24-30] mesoporous silica nanoparticles,[31] and others,[32-38] have been developed for the co-delivery of chemotherapeutics and photodynamic therapeutics. NDDSs are expected to overcome drug resistance by increased drug solubility, prolonged circulation time, programmed drug release, and sometimes improved cellular uptake.[39-47] For example, Zhu *et al.* fabricated a layered double hydroxide nanohybrid to co-deliver photosensitizers and Pt(IV) prodrugs for overcoming cisplatin resistance via synergistic chemotherapy and PDT.[35] Li *et al*. designed an intracellular acid-switchable multifunctional micelle for combinational chemo- and phototherapy of the drug-resistant tumor.[24] Chen *et al.* combined chemotherapy and phototherapy using an albumin-coordinated assembly of clearable platinum nanodots for cancer theranostics.[36] Albeit these advances, the preparation and/or formulation processes of such co-delivery systems are often complicated and multiple recipes/materials are necessary. This complexity would inevitably cause issues in scale-up manufacturing, cost, reproducibility, and biosafety. Thus, NDDSs with simple components, high biocompatibility, and easy process are highly desirable.

Poly(phosphotyrosine) (PpY) is a biomimetic polypeptide bearing a naturally occurring post-translational modification structure with good biocompatibility, enzyme responsibility, and biodegradability.[48] In our previous studies, we found that the copolymer mPEG-*block*-poly(phosphotyrosine) (mPEG-*b*-PpY) is an effective carrier for the delivery of various cargos including proteins and metallodrugs such as cisplatin (a.k.a. CDDP).[49-52] In the CDDP delivery system, the drug cisplatin functions as a crosslinker via the phosphato-platinum coordination to form the core-shell structured nanoparticle (Pt@mPEG-*b*-PpY, PtNP).[50] In addition, we previously observed weak physical association of PpY or mPEG-*b*-PpY in water despite its high charge density (Figure S1), suggesting the phenyl ring in the PpY has strong tendency to π-π stacking and hydrophobic interaction. This multimodal interacting pattern gives the polymer capability to encapsulate drug molecules with different properties.

Herein, we report a facilely fabricated NDDS, namely Pt/Ce6@mPEG-*b*-PpY (PtCeNP), for the co-delivery of cisplatin and hydrophobic photosensitizer chlorin e6 (Ce6) by simply using mPEG-*b*-PpY as the carrier (Figure 1). The ratio of Pt/Ce6 in the PtCeNP nanoparticle could be precisely regulated for an optimal synergistic effect. The physicochemical properties of PtCeNP including size, zeta potential, morphology, and release rate were studied. *In vitro* and *in vivo* antitumor experiment of the nanoparticle showed a superior safety profile and efficacy compared to parental drugs.

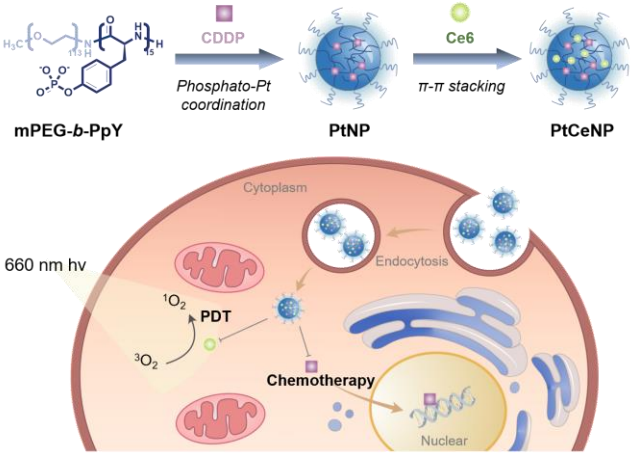

Figure 1 Cartoon illustration of the formulation and action of the mechanism of PtCeNP. CDDP and Ce6 were co-encapsulated by using mPEG-*b*-PpY as a carrier to generate the PtCeNP nanoparticle for combinational chemo-photodynamic therapy.

Results and Discussion

Preparation and ratio optimization of PtCeNP

PtNP, the precursor of PtCeNP, was firstly prepared in one step as previously described.[50] When mixing PtNP and Ce6 to make the desired PtCeNP, we found that Ce6 could be completely encapsulated into nanoparticles at various feeding ratios with no evidence of aggregation or precipitation, underlying the excellent Ce6-encapsulation capability of PtNP. It was found that a maximum of 13.6 mg/mL Ce6 could be loaded into PtCeNP using 10.5 mg mPEG-*b*-PpY_{15} under neutral conditions monitored by UV-Vis spectrophotometry, far exceeding the highest dose needed for PDT in clinical practices.

In combination therapy, the interactions between drugs may enhance efficacy and reduce side effects, or *vice versa*, that is, the conflict between drugs may result in significantly reduced efficacy or even life-threatening toxicity.[53] To quantify the synergistic effect, the concept of combination index (CI) was proposed,[54] where a value below 1.0 indicates synergy and a value equal to or larger than 1.0 suggests no synergy or even antagonism.[55] To determine the optimal Pt/Ce6 ratio in the PtCeNP, we prepared PtCeNPs with varying Pt/Ce6 ratios, tested the *in vitro* cytotoxicity against A549 cells (Figure S3, Table S1), and calculated the corresponding CI values according to the obtained IC_{50} numbers. As shown in Figure 2A, all PtCeNP tested in this study showed different levels of synergistic effect, with the smallest CI value of 0.77 achieved at a Pt/Ce6 value of 3.2/1. As such, this composition was selected for the subsequent experiments. At this ratio, as shown in Table 1 and Figure 2B, the co-delivery system PtCeNP showed a similar anticancer potency with an IC_{50} value of 29.5 μmol/L (calculated in Pt) without light, which was similar to that of PtNP (27.6 μmol/L). Since Ce6 has no obvious toxicity in dark, it is understandable that PtCeNP and PtNP were equally toxic. With light irradiation, however, the cytotoxicity of PtCeNP increased significantly due to the synergistic effect, with the IC_{50} value dropping to 11.0 μmol/L in Pt and 3.45 μmol/L in Ce6.

Characterization and *in vitro* release kinetics

The size and morphology of the nanoparticles were characterized by dynamic light scattering (DLS) and transmission

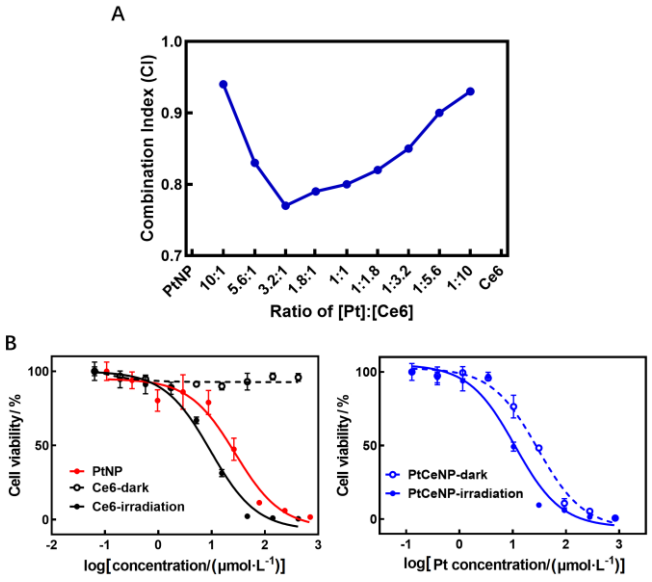

Figure 2 *In vitro* potency of PtCeNP. (A) Combination index (CI) values of PtCeNP with different ratios of cisplatin and Ce6 with 660 nm light irradiation. (B) A549 cell viability curves when treated with varying concentrations of Ce6, PtNP, or PtCeNP with or without 660 nm light irradiation. Data are presented as means ± SD (n = 3).

electron microscopy (TEM). As shown in Table 2, the hydrodynamic size of PtCeNP was slightly enlarged from PtNP's 75 to 79 nm.

TEM study confirmed the results of DLS and revealed an average diameter of the dried PtNP and PtCeNP of ~51 and 55 nm, respectively (Figures 3A, B). The zeta potential of PtCeNP increased slightly to −17.6 mV from −21.5 mV of its precursor

Table 1 IC_{50} values of Ce6, PtNP, and PtCeNP to A549 cells with or without light irradiation

	IC_{50}/(μmol·L^{-1})	
	Dark	Laser (660 nm)
Ce6	—	9.48 (In Ce6)
PtNP	27.6 (In Pt)	—

Table 2 Hydrodynamic diameter, polydispersity, and zeta potential of PtNP and PtCeNP characterized by DLS

	Diameter/nm	Polydispersity	Zeta potential/mV
PtNP	75	0.24	−21.5
PtCeNP	79	0.26	−17.5

PtNP. PtCeNP remained stable in H_2O, with no significant changes in particle sizes within 7 d (Figure 3C).

The release kinetics of nanoparticles plays a vital role in the anticancer effect of drugs. Our results showed that in DMEM with 10% FBS at 37 °C, the platinum release profile of PtCeNP was similar to that of PtNP (Figure 3D), which gradually released ~50% platinum within 48 h. We also found that PtCeNP selectively released more platinum at a substantially faster rate upon incubation with a high level of ATP but not GTP/CTP/UTP (Figure 3E), also similar to PtNP.[50] As far as the release of Ce6 was concerned, free Ce6 showed a characteristic burst release curve, whereas the release of Ce6 from PtCeNP was slower and more sustained (Figure 3F). This difference in Ce6 release implied that Ce6 distributed more homogenously in PtCeNP as compared with in water, with the latter showing obvious aggregation.

Cellular uptake of PtCeNP

Next, the cellular uptake of PtCeNP was examined from the

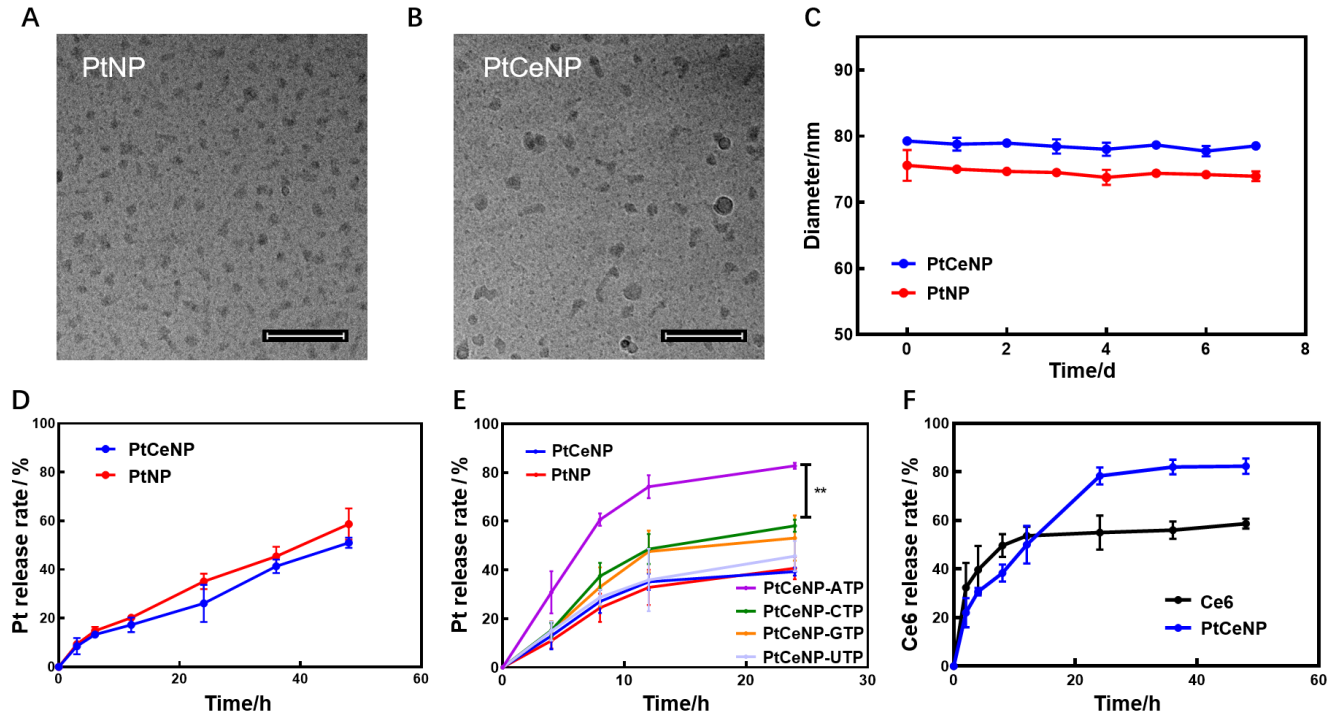

Figure 3 Physicochemical properties and release kinetics. Size and morphology of PtNP (A) and PtCeNP (B) measured by TEM (scale bar = 200 nm). (C) Changes of hydrodynamic size of PtNP and PtCeNP in H_2O within 7 d (37 °C). (D) Release kinetics of platinum from PtNP and PtCeNP in DMEM containing 10% FBS at 37 °C. (E) Release kinetics of platinum from PtCeNP in PBS containing 10 mmol/L XTP (X = A, G, C, U). (F) Release kinetics of Ce6 from a bulk Ce6 solution and PtCeNP in DMEM containing 10% FBS (MWCO = 8000 Da). All data are presented as means ± SD (n = 3). P-value was determined by two-way ANOVA analysis: $^{**}p < 0.01$.

aspects of both Ce6 and platinum. When treating A549 cells with PtCeNP or cisplatin at the same platinum concentration, ICP-MS gave higher levels of the internalized platinum for PtCeNP as compared to CDDP (Figure 4A). Meanwhile, when treating the cells with PtCeNP or free Ce6 at the same concentration (based on Ce6) for different periods of time, both flow cytometry analysis of intact cells and absorption spectrophotometry of the cell lysates showed that the cancer cells uptake more Ce6 from PtCeNP than free Ce6 (Figures 4B—D). Moreover, the cellular uptake of PtCeNP plunged significantly when the cells were pretreated with NaN_3 or 4 °C, whereas the uptake of both free cisplatin and Ce6 appeared not affected (Figures 4E—F). These results indicated that PtCeNP was mostly internalized through endocytosis, whereas both parental Ce6 and cisplatin were accumulated through energy-independent routes such as diffusion.[56]

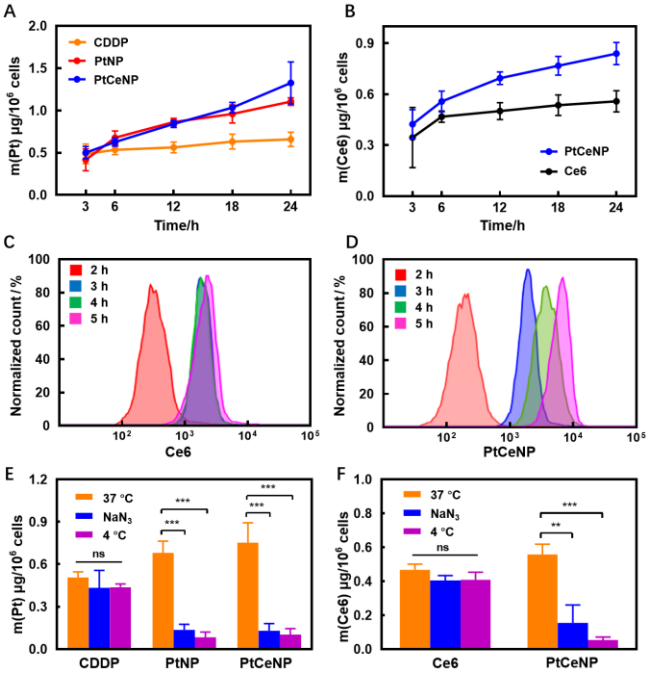

Figure 4 Cellular uptake of PtCeNP by A549 cells. (A) The levels of platinum in the cell lysates measured by ICP-MS. (B) The levels of Ce6 in the cell lysates analyzed by absorption intensity at 660 nm. (C—D) The cellular levels of Ce6 uptake measured by flow cytometry. In the above experiments, the cells were incubated with free Ce6 solution, CDDP, or PtCeNP at 37 °C for varied periods of time before analysis. (E—F) Cell uptake of platinum (E) or Ce6 (F) under various conditions (37 °C, 4 °C, or pretreated with 10 mmol/L NaN_3). In the above experiments, cells were incubated with each material under designated conditions for 6 h before the measurement of Ce6 with absorption intensity at 660 nm or platinum with ICP-MS. All data are presented as means ± SD (n = 3). P-value was determined by the two-tailed unpaired t-test: *p < 0.05, **p < 0.01, ***p < 0.001.

In vitro anticancer efficacy of PtCeNP

The intracellular delivery of Ce6 can induce ROS production upon light irradiation, thereby executing its anticancer effect. To examine the efficiency of PtCeNP in ROS generation, the intracellular ROS detection probe 2,7-dichlorodihydrofluorescein diacetate (DCFH-DA) was used to stain the cells that were treated with Ce6 or PtCeNP.[57] As shown in Figure 5, the horizontal axis represents the Ce6 content, and the vertical axis represents the DCF fluorescence level, which is directly proportional to the intracellular ROS content. While without irradiation, the ROS positive populations were less than 5% for both groups (Q2 panel), flow cytometry results indicated a remarkably higher population in ROS production upon irradiation in cells treated with PtCeNP as compared to those treated with free Ce6. The improved ROS production efficiency of PtCeNP over free Ce6 could be attributed to not only the higher uptake efficiency (Figures 4B—D), but also the more homogenous dispersion of Ce6.

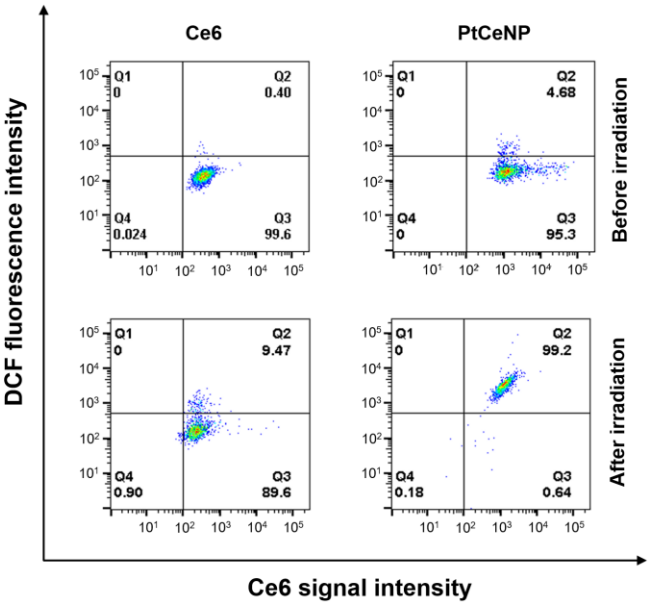

Figure 5 Intracellular ROS measurements in PtCeNP or free Ce6 treated A549 cells. The cells were incubated with designated materials at 5 μmol/L Ce6 for 6 h with or without irradiation at 660 nm for 15 min. The horizontal axis represented the Ce6 signal intensity, the vertical axis represented ROS probe signal intensity.

Next, we used the PI/FITC-Annexin V double staining to quantitatively analyze the efficacy of the drugs in inducing apoptosis of cancer cells. The results showed that the Ce6 group without light irradiation were mostly living cells, while 18% of the cells were apoptotic after irradiation. About 40%—50% of the cells treated with PtNP undergo apoptosis, and the light irradiation did not cause significant cytotoxicity change. For the cells incubated with PtCeNP, 60% of the cells were apoptotic before irradiation, while 80% of the cells were apoptotic after irradiation, which was a significant increase compared to other controls (Figure S4). These results proved that PtCeNP combined with chemotherapy and photodynamic therapy could induce cell apoptosis more effectively, demonstrating the high anticancer effect of this combinational therapy strategy.

In vivo antitumor efficacy of PtCeNP

Encouraged by the *in vitro* synergistic anticancer effect, the *in vivo* antitumor efficacy of PtCeNP was evaluated in a xenograft mouse model. BALB/c nude mice bearing subcutaneously (s.c.) implanted A549 tumors ~50 mm^3 (n = 5—7) received PBS, CDDP, PtNP, or PtCeNP every two days via tail vein injection. Subsequently, the tumor site was subjected to PDT with 660 nm light irradiation. The tumor size in PBS and CDDP groups exceeded 1500 and 700 mm^3 on day 30, respectively. PtCeNP group without light irradiation also showed excellent antitumor efficacy, in line with our previous observation.[47] To our delight, PtCeNP with light irradiation gave the best inhibition of tumor growth, with no significant tumor volume increase at the end of the study as compared to the size before treatment (Figure 6A). The volume and weight of the extracted tumors on day 30 also confirmed the superior efficacy of PtCeNP with light irradiation (Figure S5). In

terms of safety, the mice in the CDDP group experienced significant body weight loss due to its notorious systemic toxicity, whereas all other groups were well-tolerated as shown by the almost unchanged body weight (Figure 6B). In a more aggressive model containing mixed T3M4 pancreatic cancer cells and interstitial cells PSC in BALB/c-nu mice, the PtCeNP group with light irradiation again showed the best antitumor inhibition effect among all groups (Figure 6C), and was less toxic than the CDDP group (Figure 6D). The improved *in vivo* efficacy of PtCeNP echoed with the synergistic effect of combined chemotherapy and PDT observed *in vitro*. Moreover, it was found the nanocarriers enjoyed additional benefits such as prolonged blood circulation and tumor accumulation as compared to CDDP (Figures S6, S7).

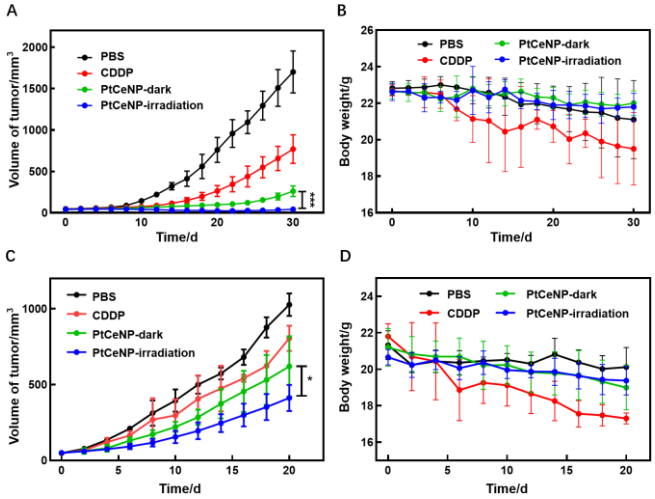

Figure 6 *In vivo* antitumor efficacy of PtCeNP. Tumor growth curve (A) and body weight change curve (B) in BALB/c-nu mice bearing xenografted A549 tumors (n = 7). The mice were administered with PBS, CDDP, or PtCeNP (with or without light irradiation) at a 1.5 mg/kg platinum dose once every two days via tail vein, and the administration was stopped on day 24. Tumor growth curve (C) and body weight change curve (D) in BALB/c-nu mice bearing xenografted T3M4 pancreatic cancer cells with interstitial PSC cells (n = 5). The mice were administered with PBS, CDDP, or PtCeNP (with or without light irradiation) at a 1.5 mg/kg platinum dose once every two days via tail vein. All data are presented as means ± SD. P-value was determined by two-way ANOVA analysis: *p < 0.05, **p < 0.01, ***p < 0.001.

Conclusions

In summary, using the block polymer mPEG-*b*-PpY as a multi-functional carrier, we successfully prepared an NDDS, PtCeNP, for the dual delivery of CDDP and Ce6. CDDP and Ce6 have distinct physicochemical properties. Thus multiple components were usually required to formulate them into one nanocarrier.[58-62] Here, we achieved this goal via only single component through a facile formulation method. The simplicity in the formulation is empowered by the unique structure characters of PpY, which contains both anionic phosphate group for metallodrug chelating and aromatic moieties for the encapsulation of PDT drugs through π-π stacking. The PtCeNP not only enhanced the solubility and bioavailability of both parental drugs, but also improved their cellular uptake, blood circulation time, and tumor accumulation. Finally, this system showed prominent synergy in antitumor effect both *in vitro* and *in vivo*. Overall, our results indicated that PpY is a biocompatible, multifunctional, and promising carrier material suitable for a variety of drugs.

Experimental

Preparation of PtNP and PtCeNP

The copolymer mPEG-*b*-PpY was synthesized according to a previous report.[50] In brief, pOEt-TyrNCA was initiated by MeO-PEG-NH_2 (M_w = 5000 Da) in anhydrous DMF to obtain the block copolymer mPEG-*b*-P(pOEt-Tyr). Bromotrimethylsilane (TMSBr) was then added to mPEG-*b*-P(pOEt-Tyr) in DCM to synthesize mPEG-*b*-PpY. The product was purified by dialysis against 100 mmol/L NaCl and subsequently ultrapure water. The degree of polymerization was determined by comparing the proton ratios of methylene units in PEG (–OCH_2CH_2–: δ = 3.7) and phenyl groups of PpY (–C_6H_4-: δ = 7.0) in ^{1}H NMR spectra (Figure S2).

PtNP, the precursor of PtCeNP, was prepared as follows. *cis*-Diamminedichloroplatinum(II) (cisplatin, CDDP) (8.0 mg, 26.6 μmol) and $AgNO_3$ (8.6 mg, 51.1 μmol) were stirred in H_2O (1.0 mL) at room temperature in dark overnight. The suspension was centrifuged at 13800 *g* for 15 min (MWCO = 3000 Da) and the supernatant was then filtered by a 0.22 μm filter to obtain an aqueous solution of *cis*-$[Pt(NH_3)_2(H_2O)_2](NO_3)_2$. The above solution was added dropwise to mPEG-*b*-PpY_{15} (30.4 mg) in H_2O (2.0 mL) at a feeding molar ratio Pt/P = 1/2. The reaction was stirred at 800 r/min and 37 °C for 24 h to yield a light blue solution. The obtained PtNP was purified and concentrated by ultrafiltration at 4000 *g* for 20 min × 3 times (MWCO = 3000 Da).

To prepare PtCeNP, Ce6 (5.0 mg, 8.4 μmol, [Pt] : [Ce6] = 3 : 1) was dissolved in 1 mL CH_3OH in a 5 mL glass vial. The solvent was removed under vacuum, and a film of Ce6 was obtained on the wall of the vial. The above PtNP solution was added to the vial and stirred at 37 °C for 24 h. The crude PtCeNP was subjected to dialysis (MWCO = 8000 Da) for 8 h, with water changed every 2 h, to remove free Ce6 to obtain pure PtCeNP. The concentration of Pt and Ce6 in PtCeNP was determined by inductively coupled plasma mass spectrometry (ICP-MS) and UV-Vis spectrophotometer, respectively.

Calculation of combination index (CI) values

A549 cells were seeded in 96-well plates at a density of 3.0 × 10^3 cells per well 24 h prior to treatment. The cells were incubated with PtCeNP with different ratios of Pt/Ce6 (9 samples, ratio from 10/1 to 1/10) at indicated concentrations. After 4 h, the medium was changed. The cells are then irradiated with 660 nm laser at a power of 5 mW·cm^{-2} for 15 min and then incubated under normal conditions for 48 h. Cell viabilities were determined by Cell-Titer-Blue Cell Viability Assay (Promega, USA). IC_{50} values were calculated using GraphPad Prism version 5.

The formula of calculating the CI values is called Chou-Talalay formula:[54]

CI (combination index) =$IC_{50}(A)_{pair}/IC_{50}(A)+IC_{50}(B)_{pair}/IC_{50}(B)$

where IC_{50} is the half inhibition concentration of individual drug A or B or paired A and B.[55]

In vitro release assay

The solution of PtCeNP at 5 mmol/L (concentration of Pt) in 1 × PBS was placed into a dialysis bag (MWCO = 8000 Da) and incubated in DMEM with 10% FBS (99.0 mL) at 37 °C. At each time point, 1.0 mL solution outside the dialysis bag was sampled. The concentration of Pt was measured by ICP-MS, and the concentration of Ce6 was analyzed by absorption intensity at 660 nm. To keep the total volume unchanged outside the dialysis bag, 1.0 mL fresh DMEM medium plus 10% FBS was added to the solution each time.

The release kinetics in the presence of XTP (X = A, G, C, U) were performed with PBS solution containing 10 mmol/L XTP instead of DMEM medium solution. All experiments were repeated in triplicates.

In vitro cell uptake assays

The *in vitro* cellular uptake assay was performed via both cell lysates quantification and flow cytometry.

For cell lysates quantification, A549 cells (5.0×10^6) were seeded in Corning 100 mm TC-Treated Culture Dishes 24 h prior to experiments. The cells were treated with Ce6 or PtCeNP at designated concentrations (2, 5, or 10 μmol/L for Ce6), and incubated for 6 h. The cells were washed with cold PBS (5.0 mL × 2), trypsinized, suspended in cold PBS (5.0 mL), and then centrifuged (1000 *g* × 5 min at 4 °C) to afford cell pellets. After another two cycles of washing and centrifugation, the final pellets were resuspended in PBS (1.0 mL) and cell numbers were counted. The suspension was evenly divided into two groups: half of the cells were digested directly with concentrated MOS nitric acid (3.0 mL) for cellular Pt uptake analysis by ICP-MS, and the other half was used for Ce6 uptake analysis by the absorption intensity at 660 nm after cell lysis. All experiments were repeated in triplicates.

For flow cytometry analysis, A549 cells (1.0×10^5/well) were seeded in a 6-well plate and incubated for 24 h at 37 °C. A fresh medium containing Ce6 or PtCeNP (5 μmol/L for Ce6) was then supplemented to the cells. After 2—5 h incubation, cells were washed with cold PBS buffer (5.0 mL × 2). The cells were then digested by Cellstripper, centrifuged, and resuspended in PBS for flow cytometry analysis.

Endocytosis inhibition experiment

A549 cells were incubated with fresh DMEM containing 10 mmol/L sodium azide (NaN_3) at 37 °C for 3 h or incubated with fresh DMEM at 4 °C for 3 h prior to treatment. Then, cells were treated with Ce6, PtNP, or PtCeNP (5 μmol/L for Ce6, 16 μmol/L for Pt). The determination procedures of cellular uptake of Ce6 and Pt were the same as the abovementioned protocol.

Intracellular ROS measurements and apoptosis analysis

A549 cells (1.0×10^5/well) were seeded in a 6-well plate and incubated for 24 h at 37 °C. A fresh medium containing Ce6, PtNP, or PtCeNP (5 μmol/L for Ce6, 16 μmol/L for Pt) was then supplemented to the cells. After 6 h incubation, the cell medium was refreshed. For light treatment, the sample was exposed to irradiation (660 nm laser at a power of 5 mW/cm^2 for 15 min), followed by rapid washing with cold PBS (5.0 mL × 2). The cells were then digested by Cellstripper, centrifuged, and resuspended in PBS.

For ROS detection, the ROS probe 2',7'-dichlorodihydrofluorescein diacetate (DCFH-DA) (5 μmol/L) was added to the cell suspensions. DCFH-DA is an oxidative stress indicator without fluorescence, which is permeable to the cell membrane. After entering the cell, it will be hydrolyzed by esterase into 2',7'-dichlorodihydrofluorescein (DCFH), which would further interact with ROS, generating the fluorescent substance 2',7'-dichlorofluorescein (DCF). The maximum excitation and emission wavelength of DCF are 480 nm and 525 nm, respectively. After 5 min incubation with DCFH-DA under dark conditions, the cells were centrifuged, washed, and resuspended (PBS, 1.0 mL). The intracellular ROS level was analyzed by flow cytometry.

For apoptosis analysis, the cells were stained according to the instructions of Annexin V-FITC Apoptosis Detection Kit. Cell apoptosis was analyzed by flow cytometry.

In vivo pharmacokinetics

BALB/c mice (*n* = 3) were treated with CDDP, PtNP, or PtCeNP at a dose of 3 mg Pt/kg weight via tail-vein injection. At designated time points, blood was withdrawn from the orbit and treated with heparin for anticlotting and centrifuged to obtain plasma. All samples were completely digested by MOS nitric acid and evaporated to dryness. The Pt concentration was measured by ICP-MS after redissolving the samples in water.

In vivo biodistribution

BALB/c-nu mice (*n* = 3) bearing A549 xenograft model were treated with CDDP, PtNP, or PtCeNP at a dose of 3 mg Pt/kg weight via tail-vein injection. Mice were sacrificed after 24 h to collect the tumors and organs. The tumors and organs were washed with cold PBS and weighted after removal of excess fluid. All samples were completely digested by MOS nitric acid and evaporated to dryness. The Pt concentration was measured by ICP-MS after redissolving the samples in water.

In vivo tumor growth inhibition

The A549 xenograft tumor model was established by subcutaneous injection of A549 cells (3.0×10^6 cells in 100 μL PBS) into the right flank of each BALB/c-nu mouse. When the tumor reached ~50 mm^3 (~10 days after tumor inoculation), the mice were randomized into 4 groups (*n* = 7). PBS, CDDP, PtNP, or PtCeNP therapy was administrated to the mice at a 1.5 mg/kg platinum dose once every two days via tail-vein injection. For photodynamic therapy, the mice in the PtCeNP group were fixed 10 h after tail-vein injection, and the tumor was irradiated (660 nm laser at a power of 5 mW/cm^2 for 1 h).

The pancreatic cancer model was established by subcutaneous injection of pancreatic cancer cells T3M4 and interstitial cells PSC at a ratio of 5 : 1 (3.0×10^6 cells total in 100 μL PBS) into the right flank of each BALB/c-nu mouse to simulate the complex tumor environment of pancreatic cancer.[63] When the tumor reached ~50 mm^3 (~8 days after tumor inoculation), the mice were randomized into 4 groups (*n* = 5). PBS, CDDP, PtNP, or PtCeNP therapy was administrated to the mice at a 1.5 mg/kg platinum dose once every two days via tail-vein injection. For photodynamic therapy, the mice in the PtCeNP group were fixed 10 h after tail-vein injection, and the tumor was irradiated (660 nm laser at a power of 5 mW/cm^2 for 1 h).

Tumor volume was calculated by the following formula:

$V = L \times W^2/2$

Relative tumor volume was calculated by the formula: $R = V/V_0$, where V_0 is the average tumor volume on day 0 (the start date of therapy). The relative body weight (R) was calculated by the formula: $R = W/W_0$, where W_0 is the body weight before administration.

Supporting Information

The supporting information for this article is available on the WWW under https://doi.org/10.1002/cjoc.202200334.

Acknowledgement

This work was supported by the National Key Research and Development Program of China (2016YFA0201400) and the National Natural Science Foundation of China for Distinguished Young Investigators (22125101).

References

[1] Gottesman, M. M.; Fojo, T.; Bates, S. E. Multidrug resistance in cancer: role of ATP–dependent transporters. *Nat. Rev. Cancer* **2002**, *2*, 48–58.

[2] Xie, P.; Wang, Y.; Wei, D.; Zhang, L.; Zhang, B.; Xiao, H.; Song, H.; Mao, X. Nanoparticle-based drug delivery systems with platinum drugs for overcoming cancer drug resistance. *J. Mater. Chem. B* **2021**, *9*, 5173–5194.

[3] Zheng, Y.; Li, Z.; Chen, H.; Gao, Y. Nanoparticle-based drug delivery systems for controllable photodynamic cancer therapy. *Eur. J. Pharm. Sci.* **2020**, *144*, 105213.

[4] Agostinis, P.; Berg, K.; Cengel, K. A.; Foster, T. H.; Girotti, A. W.; Gollnick, S. O.; Hahn, S. M.; Hamblin, M. R.; Juzeniene, A.; Kessel, D.; Korbelik, M.; Moan, J.; Mroz, P.; Nowis, D.; Piette, J.; Wilson, B. C.; Golab, J. Photodynamic therapy of cancer: An update. *CA Cancer J. Clin.* **2011**, *61*, 250–281.

[5] Yang, H.; Liu, R.; Xu, Y.; Qian, L.; Dai, Z. Photosensitizer nanoparticles boost photodynamic therapy for pancreatic cancer treatment. *Nanomicro Lett.* **2021**, *13*, 35.

[6] Xu, D.; Lin, H.; Qiu, W.; Ge, M.; Chen, Z.; Wu, C.; You, Y.; Lu, X.; Wei, C.; Liu, J.; Guo, X.; Shi, J. Hydrogen-bonded silicene nanosheets of engineered bandgap and selective degradability for photodynamic therapy. *Biomaterials* **2021**, *278*, 121172.

[7] Liang, X.; Chen, M.; Bhattarai, P.; Hameed, S.; Dai, Z. Perfluorocarbon@porphyrin nanoparticles for tumor hypoxia relief to enhance photodynamic therapy against liver metastasis of colon cancer. *ACS Nano* **2020**, *14*, 13569–13583.

[8] Zhang, Y.; Ma, J.; Wang, D.; Xu, C.; Sheng, S.; Cheng, J.; Bao, C.; Li, Y.; Tian, H. Fe-TCPP@CS nanoparticles as photodynamic and photothermal agents for efficient antimicrobial therapy. *Biomater. Sci.* **2020**, *8*, 6526–6532.

[9] Zhang, H.; Liu, K.; Li, S.; Xin, X.; Yuan, S.; Ma, G.; Yan, X. Self-assembled minimalist multifunctional theranostic nanoplatform for magnetic resonance imaging-guided tumor photodynamic therapy. *ACS Nano* **2018**, *12*, 8266–8276.

[10] Fan, W.; Yung, B.; Huang, P.; Chen, X. Nanotechnology for multimodal synergistic cancer therapy. *Chem. Rev.* **2017**, *117*, 13566–13638.

[11] Ni, W.; Wu, J.; Fang, H.; Feng, Y.; Hu, Y.; Lin, L.; Chen, J.; Chen, F.; Tian, H. Photothermal-chemotherapy enhancing tumor immunotherapy by multifunctional metal–organic framework based drug delivery system. *Nano Lett.* **2021**, *21*, 7796–7805.

[12] Canti, G.; Nicolin, A.; Cubeddu, R.; Taroni, P.; Bandieramonte, G.; Valentini, G. Antitumor efficacy of the combination of photodynamic therapy and chemotherapy in murine tumors. *Cancer Lett.* **1998**, *125*, 39–44.

[13] Kemp, J. A.; Shim, M. S.; Heo, C. Y.; Kwon, Y. J. "Combo" nanomedicine: Co-delivery of multi-modal therapeutics for efficient, targeted, and safe cancer therapy. *Adv. Drug Del. Rev.* **2016**, *98*, 3–18.

[14] Chatterjee, D. K.; Fong, L. S.; Zhang, Y. Nanoparticles in photodynamic therapy: An emerging paradigm. *Adv. Drug Del. Rev.* **2008**, *60*, 1627–1637.

[15] Liu, M.; Meng, J.; Bao, W.; Liu, S.; Wei, W.; Ma, G.; Tian, Z. Single-chromophore-based therapeutic agent enables green-light-triggered chemotherapy and simultaneous photodynamic therapy to cancer cells. *ACS Appl. Bio Mater.* **2019**, *2*, 3068–3076.

[16] Mignani, S.; Bryszewska, M.; Klajnert-Maculewicz, B.; Zablocka, M.; Majoral, J.-P. Advances in combination therapies based on nanoparticles for efficacious cancer treatment: an analytical report. *Biomacromolecules* **2015**, *16*, 1–27.

[17] Guo, Z.; Zou, Y.; He, H.; Rao, J.; Ji, S.; Cui, X.; Ke, H.; Deng, Y.; Yang, H.; Chen, C.; Zhao, Y.; Chen, H. Bifunctional platinated nanoparticles for photoinduced tumor ablation. *Adv. Mater.* **2016**, *28*, 10155–10164.

[18] Li, T.-F.; Xu, H.-Z.; Xu, Y.-H.; Yu, T.-T.; Tang, J.-M.; Li, K.; Wang, C.; Peng, X.-C.; Li, Q.-R.; Sang, X.-Y.; Zheng, M.-Y.; Liu, Y.; Zhao, L.; Chen, X. Efficient delivery of chlorin e6 by polyglycerol-coated iron oxide nanoparticles with conjugated doxorubicin for enhanced photodynamic therapy of melanoma. *Mol. Pharm.* **2021**, *18*, 3601–3615.

[19] Li, Y.; Liu, G.; Ma, J.; Lin, J.; Lin, H.; Su, G.; Chen, D.; Ye, S.; Chen, X.; Zhu, X.; Hou, Z. Chemotherapeutic drug-photothermal agent co-self-assembling nanoparticles for near-infrared fluorescence and photoacoustic dual-modal imaging-guided chemo-photothermal synergistic therapy. *J. Control. Release* **2017**, *258*, 95–107.

[20] Yu, X. Z.; Zhu, W.; Di, Y.; Gu, J.; Guo, Z.; Li, H.; Fu, D.; Jin, C. Triple-functional albumin-based nanoparticles for combined chemotherapy and photodynamic therapy of pancreatic cancer with lymphatic metastases. *Int. J. Nanomedicine* **2017**, *12*, 6771–6785.

[21] Fan, L.; Zhao, S.; Yang, Q.; Tan, J.; Song, C.; Wu, H. Ternary cocktail nanoparticles for sequential chemo-photodynamic therapy. *J. Exp. Clin. Cancer Res.* **2017**, *36*, 119.

[22] You, J.; Zhang, P.; Hu, F.; Du, Y.; Yuan, H.; Zhu, J.; Wang, Z.; Zhou, J.; Li, C. Near-infrared light-sensitive liposomes for the enhanced photothermal tumor treatment by the combination with chemotherapy. *Pharm. Res.* **2014**, *31*, 554–565.

[23] Panikar, S. S.; Ramírez-García, G.; Vallejo-Cardona, A. A.; Banu, N.; Patrón-Soberano, O. A.; Cialla-May, D.; Camacho-Villegas, T. A.; de la Rosa, E. Novel anti-HER2 peptide-conjugated theranostic nanoliposomes combining NaYF4: Yb,Er nanoparticles for NIR-activated bioimaging and chemo-photodynamic therapy against breast cancer. *Nanoscale* **2019**, *11*, 20598–20613.

[24] Wang, T.; Wang, D.; Yu, H.; Wang, M.; Liu, J.; Feng, B.; Zhou, F.; Yin, Q.; Zhang, Z.; Huang, Y.; Li, Y. Intracellularly acid-switchable multifunctional micelles for combinational photo/chemotherapy of the drug-resistant tumor. *ACS Nano* **2016**, *10*, 3496–3508.

[25] Ma, Q.; Zhao, Y.; Guan, Q.; Zhao, Y.; Zhang, H.; Ding, Z.; Wang, Q.; Wu, Y.; Liu, M.; Han, J. Amphiphilic block polymer-based self-assembly of high payload nanoparticles for efficient combinatorial chemo-photodynamic therapy. *Drug Deliv.* **2020**, *27*, 1656–1666.

[26] Gao, D.; Lo, P.-C. Polymeric micelles encapsulating pH-responsive doxorubicin prodrug and glutathione-activated zinc(II) phthalocyanine for combined chemotherapy and photodynamic therapy. *J. Control. Release* **2018**, *282*, 46–61.

[27] Dag, A.; Cakilkaya, E.; Omurtag Ozgen, P. S.; Atasoy, S.; Yigit Erdem, G.; Cetin, B.; Çavuş Kokuroğlu, A.; Gürek, A. G. Phthalocyanine-conjugated glyconanoparticles for chemo-photodynamic combination therapy. *Biomacromolecules* **2021**, *22*, 1555–1567.

[28] Kim, D. H.; Hwang, H. S.; Na, K. Photoresponsive micelle-incorporated doxorubicin for chemo-photodynamic therapy to achieve synergistic antitumor effects. *Biomacromolecules* **2018**, *19*, 3301–3310.

[29] Chen, Y.; Ren, J.; Tian, D.; Li, Y.; Jiang, H.; Zhu, J. Polymer–upconverting nanoparticle hybrid micelles for enhanced synergistic chemo–photodynamic therapy: effects of emission–absorption spectral match. *Biomacromolecules* **2019**, *20*, 4044–4052.

[30] Zhu, R.; He, H.; Liu, Y.; Cao, D.; Yan, J.; Duan, S.; Chen, Y.; Yin, L. Cancer-selective bioreductive chemotherapy mediated by dual hypoxia-responsive nanomedicine upon photodynamic therapy-induced hypoxia aggravation. *Biomacromolecules* **2019**, *20*, 2649–2656.

[31] Cheng, Y.-J.; Hu, J.-J.; Qin, S.-Y.; Zhang, A.-Q.; Zhang, X.-Z. Recent advances in functional mesoporous silica-based nanoplatforms for combinational photo-chemotherapy of cancer. *Biomaterials* **2020**, *232*, 119738.

[32] Liu, J.; Yang, G.; Zhu, W.; Dong, Z.; Yang, Y.; Chao, Y.; Liu, Z. Light-controlled drug release from singlet-oxygen sensitive nanoscale coordination polymers enabling cancer combination therapy. *Biomaterials* **2017**, *146*, 40–48.

[33] Wan, G.; Chen, B.; Li, L.; Wang, D.; Shi, S.; Zhang, T.; Wang, Y.; Zhang, L.; Wang, Y. Nanoscaled red blood cells facilitate breast cancer treatment by combining photothermal/photodynamic therapy and chemotherapy. *Biomaterials* **2018**, *155*, 25–40.

[34] Wang, Y.; Wei, G.; Zhang, X.; Huang, X.; Zhao, J.; Guo, X.; Zhou, S. Multistage targeting strategy using magnetic composite nanoparticles for synergism of photothermal therapy and chemotherapy. *Small* **2018**, *14*, 1702994.

[35] Wang, Z.; Ma, R.; Yan, L.; Chen, X.; Zhu, G. Combined chemotherapy and photodynamic therapy using a nanohybrid based on layered double hydroxides to conquer cisplatin resistance. *Chem. Commun.* **2015**, *51*, 11587–11590.

[36] Tang, Y.; Yang, T.; Wang, Q.; Lv, X.; Song, X.; Ke, H.; Guo, Z.; Huang, X.; Hu, J.; Li, Z.; Yang, P.; Yang, X.; Chen, H. Albumin-coordinated assembly of clearable platinum nanodots for photo-induced cancer theranostics. *Biomaterials* **2018**, *154*, 248–260.

[37] Dai, X.; Zhang, B.; Zhou, W.; Liu, Y. High-efficiency synergistic effect of supramolecular nanoparticles based on cyclodextrin prodrug on cancer therapy. *Biomacromolecules* **2020**, *21*, 4998–5007.

[38] Pandya, A. D.; Øverbye, A.; Sahariah, P.; Gaware, V. S.; Høgset, H.; Masson, M.; Høgset, A.; Mælandsmo, G. M.; Skotland, T.; Sandvig, K.;

Iversen, T.-G. Drug-loaded photosensitizer-chitosan nanoparticles for combinatorial chemo- and photodynamic-therapy of cancer. *Biomacromolecules* **2020**, *21*, 1489–1498.

[39] Ding, J.; Chen, J.; Gao, L.; Jiang, Z.; Zhang, Y.; Li, M.; Xiao, Q.; Lee, S. S.; Chen, X. Engineered nanomedicines with enhanced tumor penetration. *Nano Today* **2019**, *29*, 100800.

[40] Guo, Z.; Lin, L.; Hao, K.; Wang, D.; Liu, F.; Sun, P.; Yu, H.; Tang, Z.; Chen, M.; Tian, H.; Chen, X. Helix self-assembly behavior of amino acid-modified camptothecin prodrugs and its antitumor effect. *ACS Appl. Mater. Interfaces* **2020**, *12*, 7466–7476.

[41] Chen, J.; Zhu, Y.; Wu, C.; Shi, J. Nanoplatform-based cascade engineering for cancer therapy. *Chem. Soc. Rev.* **2020**, *49*, 9057–9094.

[42] Zhao, L.; Shen, G.; Ma, G.; Yan, X. Engineering and delivery of nanocolloids of hydrophobic drugs. *Adv. Colloid Interface Sci.* **2017**, *249*, 308–320.

[43] Bu, L.-L.; Yan, J.; Wang, Z.; Ruan, H.; Chen, Q.; Gunadhi, V.; Bell, R. B.; Gu, Z. Advances in drug delivery for post-surgical cancer treatment. *Biomaterials* **2019**, *219*, 119182.

[44] Wang, L.; Yu, Y.; Wei, D.; Zhang, L.; Zhang, X.; Zhang, G.; Ding, D.; Xiao, H.; Zhang, D. A systematic strategy of combinational blow for overcoming cascade drug resistance via NIR-light-triggered hyperthermia. *Adv. Mater.* **2021**, *33*, 2100599.

[45] Wei, D.; Yu, Y.; Zhang, X.; Wang, Y.; Chen, H.; Zhao, Y.; Wang, F.; Rong, G.; Wang, W.; Kang, X.; Cai, J.; Wang, Z.; Yin, J.-Y.; Hanif, M.; Sun, Y.; Zha, G.; Li, L.; Nie, G.; Xiao, H. Breaking the intracellular redox balance with diselenium nanoparticles for maximizing chemotherapy efficacy on patient-derived xenograft models. *ACS Nano* **2020**, *14*, 16984–16996.

[46] Wang, Y.; Jiang, Y.; Wei, D.; Singh, P.; Yu, Y.; Lee, T.; Zhang, L.; Mandl, H. K.; Piotrowski-Daspit, A. S.; Chen, X.; Li, F.; Li, X.; Cheng, Y.; Josowitz, A.; Yang, F.; Zhao, Y.; Wang, F.; Zhao, Z.; Huttner, A.; Bindra, R. S.; Xiao, H.; Mark Saltzman, W. Nanoparticle-mediated convection-enhanced delivery of a DNA intercalator to gliomas circumvents temozolomide resistance. *Nat. Biomed. Eng.* **2021**, *5*, 1048–1058.

[47] Yu, S.; Wei, S.; Liu, L.; Qi, D.; Wang, J.; Chen, G.; He, W.; He, C.; Chen, X.; Gu, Z. Enhanced local cancer therapy using a CA4P and CDDP co-loaded polypeptide gel depot. *Biomater. Sci.* **2019**, *7*, 860–866.

[48] Sun, Y.; Hou, Y.; Zhou, X.; Yuan, J.; Wang, J.; Lu, H. Controlled synthesis and enzyme-induced hydrogelation of poly(l-phosphotyrosine) via ring-opening polymerization of α-amino acid *N*-carboxyanhydride. *ACS Macro Lett.* **2015**, *4*, 1000–1003.

[49] Zhou, H.; Wang, Y.; Lu, H. Intracellular delivery of His-tagged proteins via a hybrid organic–inorganic nanoparticle. *Polym. J.* **2021**, *53*, 1259–1267.

[50] Hou, Y.; Wang, Y.; Wang, R.; Bao, W.; Xi, X.; Sun, Y.; Yang, S.; Wei, W.; Lu, H. Harnessing phosphato-platinum bonding induced supramolecular assembly for systemic cisplatin delivery. *ACS Appl. Mater. Interfaces* **2017**, *9*, 17757–17768.

[51] Li, S. L.; Hou, Y.; Hu, Y.; Yu, J.; Wei, W.; Lu, H. Phosphatase-triggered cell-selective release of a Pt(iv)-backboned prodrug-like polymer for an improved therapeutic index. *Biomater. Sci.* **2017**, *5*, 1558–1566.

[52] Li, S. L.; Wang, Y.; Zhang, J.; Wei, W.; Lu, H. Targeted delivery of a guanidine-pendant Pt(iv)-backboned poly-prodrug by an anisamide-functionalized polypeptide. *J. Mater. Chem. B* **2017**, *5*, 9546–9557.

[53] Wu, X.; Zhou, L.; Su, Y.; Dong, C.-M. Plasmonic, targeted, and dual drugs-loaded polypeptide composite nanoparticles for synergistic cocktail chemotherapy with photothermal therapy. *Biomacromolecules* **2016**, *17*, 2489–2501.

[54] Chou, T.-C.; Talalay, P. Quantitative analysis of dose-effect relationships: the combined effects of multiple drugs or enzyme inhibitors. *Adv. Enzyme Regul.* **1984**, *22*, 27–55.

[55] Ma, L.; Kohli, M.; Smith, A. Nanoparticles for combination drug therapy. *ACS Nano* **2013**, *7*, 9518–9525.

[56] Scarmato, P.; Durand, G.; Agneray, J.; Feger, J. Inhibitory effect of sodium arsenite and azide on asialoglycoprotein receptor mediated endocytosis in suspended rat hepatocytes. *Biol. Cell* **1986**, *56*, 255–258.

[57] LeBel, C. P.; Ischiropoulos, H.; Bondy, S. C. Evaluation of the probe 2',7'-dichlorofluorescin as an indicator of reactive oxygen species formation and oxidative stress. *Chem. Res. Toxicol.* **1992**, *5*, 227–231.

[58] Chen, Y.; Zhang, L.; Li, F.; Sheng, J.; Xu, C.; Li, D.; Yu, H.; Liu, W. Combination of chemotherapy and photodynamic therapy with oxygen self-supply in the form of mutual assistance for cancer therapy. *Int. J. Nanomedicine* **2021**, *16*, 3679–3694.

[59] You, C.; Gao, Z.; Wang, M.; Wu, H.; An, P.; Wang, S.; Sun, Y.; Sun, B.; Zhang, X. Cisplatin and Ce6 loaded polyaniline nanoparticles: An efficient near-infrared light mediated synergistic therapeutic agent. *Mater. Sci. Eng. C* **2019**, *95*, 183–191.

[60] Zhang, W.; Shen, J.; Su, H.; Mu, G.; Sun, J.-H.; Tan, C.-P.; Liang, X.-J.; Ji, L.-N.; Mao, Z.-W. Co-delivery of cisplatin prodrug and Chlorin e6 by mesoporous silica nanoparticles for chemo-photodynamic combination therapy to combat drug resistance. *ACS Appl. Mater. Interfaces* **2016**, *8*, 13332–13340.

[61] Song, C.; Tang, C.; Xu, W.; Ran, J.; Wei, Z.; Wang, Y.; Zou, H.; Cheng, W.; Cai, Y.; Han, W. Hypoxia-targeting multifunctional nanoparticles for sensitized chemotherapy and phototherapy in head and neck squamous cell carcinoma. *Int. J. Nanomedicine* **2020**, *15*, 347–361.

[62] Wang, M.; You, C.; Gao, Z.; Wu, H.; Sun, B.; Zhu, X.; Chen, R. A dual-targeting strategy for enhanced drug delivery and synergistic therapy based on thermosensitive nanoparticles. *J. Biomater. Sci. Polym. Ed.* **2018**, *29*, 1360–1374.

[63] Wang, F.; Ma, L.; Zhang, Z.; Liu, X.; Gao, H.; Zhuang, Y.; Yang, P.; Kornmann, M.; Tian, X.; Yang, Y. Hedgehog signaling regulates epithelial-mesenchymal transition in pancreatic cancer stem-like cells. *J. Cancer* **2016**, *7*, 408–417.

Manuscript received: June 3, 2022
Manuscript revised: July 11, 2022
Manuscript accepted: July 12, 2022
Accepted manuscript online: July 14, 2022
Version of record online: XXXX, 2022

The Authors

Left to Right: (Top) Haisen Zhou, Yaoyi Wang, Yingqin Hou, (Bottom) Zhengkui Zhang, Qi Wang, Xiaodong Tian, Hua Lu